Poloidal motion of trapped particle orbits in real-space coordinates

V. V. Nemov,[1] S. V. Kasilov,[1] W. Kernbichler,[2] and G. O. Leitold[2]
[1]*Institute of Plasma Physics, National Science Center, "Kharkov Institute of Physics and Technology," Akademicheskaya str. 1, 61108 Kharkov, Ukraine*
[2]*Association EURATOM-ÖAW, Institut für Theoretische Physik-Computational Physics, Technische Universität Graz, Petersgasse 16, A-8010 Graz, Austria*

(Received 28 December 2007; accepted 31 March 2008; published online 9 May 2008)

The bounce averaged poloidal drift velocity of trapped particles in stellarators is an important quantity in the framework of optimization of stellarators because it allows us to analyze the possibility for closure of contours of the second adiabatic invariant and therefore for improvement of α-particle confinement in such a device. Here, a method is presented to compute such a drift velocity directly in real space coordinates through integration along magnetic field lines. This has the advantage that one is not limited to the usage of magnetic coordinates and can use the magnetic field produced by coil currents and more importantly also results of three-dimensional magnetohydrodynamic finite beta equilibrium codes, such as PIES [A. H. Reiman and H. S. Greenside, J. Comput. Phys. **75**, 423 (1988)] and HINT [Y. Suzuki *et al.*, Nucl. Fusion **46**, L19 (2006)]. © *2008 American Institute of Physics*. [DOI: 10.1063/1.2912456]

I. INTRODUCTION

Theoretical and numerical studies of charged particle losses are important for assessment of general confinement properties of stellarator devices.[1] In the long-mean-free-path regime which is characteristic of thermonuclear plasma applications, the particle confinement in stellarators (collisionless confinement) is mainly determined by confinement of trapped particle orbits. Those particles can be trapped within one magnetic field ripple as well as within several neighboring magnetic field ripples. Here two types of drift motion are important: (i) the missing (axi-)symmetry in stellarators causes the ∇B-drift of particle orbits which describes the radial drift across magnetic surfaces, and (ii) the poloidal motion of particle orbits. A detailed study of these effects allows one to obtain appropriate criteria for improving the particle confinement which require less computer resources than codes for direct computations of guiding center drift equations (e.g., Monte Carlo codes for computation of collisionless α-particle confinement).

It is well known, that a sufficiently large poloidal drift velocity of trapped particles promotes the formation of poloidally closed contours of the second adiabatic invariant, $J_\parallel = \oint v_\parallel ds$. This, in turn, leads to an essential decrease of trapped particle losses, in particular, α-particle losses (see, e.g., Ref. 2); and vice versa trapped particles with a small poloidal drift can create poloidally unclosed contours of $J_\parallel$ and the presence of such particles is undesirable. Recently, in Ref. 3 the possibility of a numerical analysis of the bounce-averaged poloidal drift of trapped particles has been studied in stellarator magnetic fields given in magnetic coordinates. In the present work, an analogous study is carried out for stellarator magnetic fields given in real-space coordinates. Using this approach, the trapped particle motion can be analyzed for magnetic fields produced directly by electrical currents in the coils of the device as well as for magnetic fields calculated in real space coordinates by three-dimensional magnetohydrodynamic (MHD) finite beta equilibrium codes such as PIES[4] and HINT.[5]

The paper is organized as follows: Sec. II describes the derivation of formulas for the velocity of the bounce-averaged poloidal drift of trapped particles based on integration along magnetic field lines in a given magnetic field. In particular, these formulas contain gradients of integrals of differential equations of field lines. The computation of these gradients is discussed in Sec. III. In Sec. IV some additional questions related to the application of the obtained formulas are discussed. In particular, flux surface averaged quantities which characterize the poloidal drift of trapped particles are obtained. As examples, results for three stellarator real-space magnetic configurations are presented in Sec. V, namely, for the Compact Helical System[6] (CHS) heliotron/torsatron configuration, for the Uragan-2M[7] (U-2M) torsatron, and for the Wendelstein 7-X[1] (W7-X) Helias-type configuration. Some conclusions are presented in Sec. VI.

II. BASIC EQUATIONS

Here, a Clebsch representation of the magnetic field $\mathbf{B}$, $\mathbf{B}=\nabla\psi\times\nabla\theta_0$, is used where ψ labels a regular or island magnetic surface and θ_0 is in general a multivalued function of coordinates which labels a given field line on a magnetic surface. As the third coordinate, φ is used which is counted along the magnetic field line. In addition, the equations for particle motion (3.41) of Ref. 8 are used which had been applied in Ref. 8 to the derivation of the second adiabatic invariant. In $(\psi, \theta_0, \varphi)$ notation these equations are given as

$$\frac{d\psi}{dt} = \frac{cv_\parallel}{eB\sqrt{g}}\left[\frac{\partial}{\partial\theta_0}(mv_\parallel h_\varphi) - \frac{\partial}{\partial\varphi}(mv_\parallel h_{\theta_0})\right], \tag{1}$$

$$\frac{d\theta_0}{dt} = \frac{cv_\parallel}{eB\sqrt{g}}\left[\frac{\partial}{\partial\varphi}(mv_\parallel h_\psi) - \frac{\partial}{\partial\psi}(mv_\parallel h_\varphi)\right], \tag{2}$$

$$\frac{d\varphi}{dt} \approx v_{\parallel} h^{\varphi}, \tag{3}$$

where $\sqrt{g}=1/(\nabla\psi\times\nabla\theta_0\cdot\nabla\varphi)$, $h^{\psi}=h^{\theta_0}=0$, $h^{\varphi}=1/(B\sqrt{g})$, h^{ψ}, h^{θ_0}, and h^{φ} are the contravariant components of the unit vector $\mathbf{h}=\mathbf{B}/\mathrm{B}$, h_{ψ}, h_{θ_0}, and h_{φ} are the covariant components of this vector.

The poloidal motion of trapped particles is characterized by the increment of θ_0, $\Delta\theta_0$, during one bounce period. A peculiarity of the coordinates (ψ,θ_0,φ) is that in toroidal geometry $\nabla\theta_0$ is not single valued. This makes problems in the case of simultaneous calculations for a variety of trapped particles distributed along the magnetic field line. To avoid these problems, a further transition is performed from θ_0 to a variable θ connected with θ_0 by the relationship

$$\theta = \theta_0 + \chi\varphi, \tag{4}$$

with $\chi=\chi(\psi)$ and $\nabla\theta$ being single valued quantities. Actually, this change is analogous to the case of transition from nonperiodic magnetic coordinates to periodic ones in Ref. 9. The quantity χ is a linear function of the rotational transform of magnetic field lines, ι. To ensure a single valued characteristic of $\nabla\theta$, conditions for χ can be found in the following way. From Eq. (4), one finds

$$\nabla\theta_0 = \nabla\theta - \chi\nabla\varphi - \varphi\chi'\nabla\psi, \tag{5}$$

where prime denotes the derivative with respect to ψ. The scalar product of Eq. (5) and $\nabla\psi$ gives

$$\nabla\theta_0\cdot\nabla\psi = \nabla\theta\cdot\nabla\psi - \chi\nabla\varphi\cdot\nabla\psi - \varphi\chi'|\nabla\psi|^2. \tag{6}$$

Since $(\nabla\theta\cdot\nabla\psi-\chi\nabla\varphi\cdot\nabla\psi)/|\nabla\psi|^2$ is finite, χ' can be found from Eq. (6) as

$$\chi' = -\lim_{\varphi\to\infty}\frac{1}{\varphi}\frac{\nabla\theta_0\cdot\nabla\psi}{|\nabla\psi|^2}. \tag{7}$$

For a magnetic field given in real-space coordinates the computation of $\nabla\psi$ and $\nabla\theta_0$ in Eq. (7) and in the following expressions is performed using the technique described in the next section. It should be noted that for real-space representations of $\mathbf{B}$ the variable θ is only counted in the poloidal direction but its period differs in general from 2π.

From the relation between θ and θ_0, Eq. (4) one can derive

$$\frac{d\theta}{dt} = \frac{d\theta_0}{dt} + \chi\frac{d\varphi}{dt} + \varphi\chi'\frac{d\psi}{dt}. \tag{8}$$

Substituting Eqs. (1)–(3) into Eq. (8) and integrating with respect to t one finds

$$\Delta\theta = \chi\Delta\varphi - \frac{c}{e}\int\left[\frac{\partial}{\partial\psi}(mv_{\parallel}h_{\varphi}) - \varphi\chi'\frac{\partial}{\partial\theta_0}(mv_{\parallel}h_{\varphi})\right]d\varphi + \frac{c}{e}\int\frac{\partial}{\partial\varphi}(mv_{\parallel}h_{\psi})d\varphi - \chi'\frac{c}{e}\int\varphi\frac{\partial}{\partial\varphi}(mv_{\parallel}h_{\theta_0})d\varphi. \tag{9}$$

Taking the integrals in Eq. (9) over an interval of φ corresponding to one bounce period, τ_b, and noting that for this interval $\Delta\varphi=0$ one obtains

$$\Delta\hat{\theta} = -\frac{c}{e}\oint\left[\frac{\partial}{\partial\psi}(mv_{\parallel}h_{\varphi}) - \varphi\chi'\frac{\partial}{\partial\theta_0}(mv_{\parallel}h_{\varphi})\right]d\varphi + \chi'\frac{c}{e}\oint mv_{\parallel}h_{\theta_0}d\varphi. \tag{10}$$

The covariant components of $\mathbf{h}$ can be given in the form

$$h_{\psi} = \mathbf{h}\cdot\mathbf{e}_{\psi} = \mathbf{h}\cdot(\nabla\theta_0\times\nabla\varphi)\sqrt{g},$$

$$h_{\theta_0} = \mathbf{h}\cdot\mathbf{e}_{\theta_0} = \mathbf{h}\cdot(\nabla\varphi\times\nabla\psi)\sqrt{g}, \tag{11}$$

$$h_{\varphi} = \mathbf{h}\cdot\mathbf{e}_{\varphi} = B/B^{\varphi} = 1/h^{\varphi},$$

using the contravariant basis set

$$\mathbf{e}_{\psi} = \sqrt{g}(\nabla\theta_0\times\nabla\varphi),$$

$$\mathbf{e}_{\theta_0} = \sqrt{g}(\nabla\varphi\times\nabla\psi), \tag{12}$$

$$\mathbf{e}_{\varphi} = \sqrt{g}(\nabla\psi\times\nabla\theta_0),$$

by which the infinitesimal distance, $d\mathbf{r}$,

$$d\mathbf{r} = \mathbf{e}_{\psi}d\psi + \mathbf{e}_{\theta_0}d\theta_0 + \mathbf{e}_{\varphi}d\varphi, \tag{13}$$

is determined.

From

$$\nabla(v_{\parallel}h_{\varphi}) = \frac{\partial(v_{\parallel}h_{\varphi})}{\partial\psi}\nabla\psi + \frac{\partial(v_{\parallel}h_{\varphi})}{\partial\theta_0}\nabla\theta_0 + \frac{\partial(v_{\parallel}h_{\varphi})}{\partial\varphi}\nabla\varphi \tag{14}$$

and Eq. (12), one finds

$$\mathbf{e}_{\psi}\cdot\nabla(v_{\parallel}h_{\varphi}) = \frac{\partial(v_{\parallel}h_{\varphi})}{\partial\psi}, \quad \mathbf{e}_{\theta_0}\cdot\nabla(v_{\parallel}h_{\varphi}) = \frac{\partial(v_{\parallel}h_{\varphi})}{\partial\theta_0}, \tag{15}$$

and

$$\frac{\partial}{\partial\psi}(v_{\parallel}h_{\varphi}) - \chi'\varphi\frac{\partial}{\partial\theta_0}(v_{\parallel}h_{\varphi}) = (\mathbf{e}_{\psi} - \chi'\varphi\mathbf{e}_{\theta_0})\cdot\nabla(v_{\parallel}h_{\varphi}) = \sqrt{g}\nabla(v_{\parallel}B/B^{\varphi})\times(\nabla\theta_0 + \chi'\varphi\nabla\psi)\cdot\nabla\varphi. \tag{16}$$

Note that the last formula actually represents the $\partial(v_{\parallel}h_{\varphi})/\partial\psi$ derivative calculated in (ψ,θ,φ) coordinates. Substituting Eq. (16) into Eq. (10) and taking into account that $v_{\parallel}(\mathbf{r},w,J_{\perp})=\sigma\sqrt{v^2-J_{\perp}B}$, $v^2=2(w-e\Phi)/m$, $J_{\perp}=v_{\perp}^2/B$, $\sigma=\pm1$ and $\nabla v_{\parallel}=-(2e\nabla\Phi/m+J_{\perp}\nabla B)/(2v_{\parallel})$, after some transformation one obtains $\Delta\hat{\theta}$ in the form

$$\Delta\hat{\theta} = \Delta\hat{\theta}_{\nabla B} + \Delta\hat{\theta}_{E} + \Delta\hat{\theta}_{v_{\parallel}}, \tag{17}$$

with

$$\Delta\hat{\theta}_{\nabla B} = \frac{mc}{e}\oint\frac{d\varphi}{B^{\varphi}}\frac{(v_{\parallel}^2 + (1/2)J_{\perp}B)}{v_{\parallel}}\frac{\partial B}{\partial\psi}, \tag{18}$$

$$\Delta\hat{\theta}_{E} = c\Phi'\oint\frac{B}{v_{\parallel}}\frac{d\varphi}{B^{\varphi}} = c\Phi'\tau_b, \tag{19}$$

$$\Delta\hat{\theta}_{v_\parallel} = \frac{mc}{e}\oint \frac{d\varphi}{B^\varphi} v_\parallel \left[\chi'(\nabla\psi\times\mathbf{h})\cdot\nabla\varphi - \left(2\frac{\partial B}{\partial\psi} - \frac{B}{B^\varphi}\frac{\partial B^\varphi}{\partial\psi}\right)\right], \tag{20}$$

where

$$\frac{\partial B}{\partial\psi} = \frac{1}{B^\varphi}\nabla B\times(\nabla\theta_0 + \chi'\varphi\nabla\psi)\cdot\nabla\varphi, \tag{21}$$

$$\frac{\partial B^\varphi}{\partial\psi} = \frac{1}{B^\varphi}\nabla B^\varphi\times(\nabla\theta_0 + \chi'\varphi\nabla\psi)\cdot\nabla\varphi, \tag{22}$$

and $\nabla\theta_0+\chi'\varphi\nabla\psi$ is a single valued quantity in the case of χ' defined by Eq. (7). The equality $d\varphi/B^\varphi = ds/B$ has been used in Eq. (19) with s being the length along the magnetic field line.

Every trapped particle is trapped within a certain segment of the magnetic field line limited by the turning points $s_j^{\min}$ and $s_j^{\max}$, where j is numbering the segments along the magnetic field line. With this definition one can express the bounce time $\tau_{b,j}$ as

$$\tau_{b,j} = \oint_{(j)} \frac{d\varphi}{B^\varphi}\frac{B}{v_\parallel} = \oint_{(j)}\frac{\mathrm{d}s}{v_\parallel} = 2\int_{s_j^{\min}}^{s_j^{\max}}\frac{\mathrm{d}s}{|v_\parallel|}. \tag{23}$$

According to the equalities

$$v_\parallel = -\frac{\partial}{\partial J_\perp}\left(\frac{2v_\parallel^3}{3B}\right), \quad \frac{1}{v_\parallel} = -\frac{2}{B}\frac{\partial v_\parallel}{\partial J_\perp}, \tag{24}$$

$$\frac{v_\parallel^2 + (1/2)J_\perp B}{v_\parallel} = -\frac{\partial}{\partial J_\perp}\left[\frac{1}{B}v_\parallel\left(v^2 + \frac{1}{3}v_\parallel^2\right)\right], \tag{25}$$

expressions (18), (20), and (23) can be presented as

$$\Delta\hat{\theta}_{\nabla B} = -\frac{mc}{e}\frac{\partial G_j}{\partial J_\perp}, \tag{26}$$

$$\Delta\hat{\theta}_{v_\parallel} = -\frac{mc}{e}\frac{\partial V_j}{\partial J_\perp}, \tag{27}$$

$$\tau_{b,j} = -2\frac{\partial I_j}{\partial J_\perp}, \quad I_j = 2\int_{s_j^{\min}}^{s_j^{\max}}\frac{\mathrm{d}s}{B}|v_\parallel|, \tag{28}$$

with

$$G_j = 2\int_{s_j^{\min}}^{s_j^{\max}}\frac{\mathrm{d}s}{B^2}\frac{\partial B}{\partial\psi}|v_\parallel|\left(v^2 + \frac{1}{3}v_\parallel^2\right), \tag{29}$$

$$V_j = \frac{4}{3}\int_{s_j^{\min}}^{s_j^{\max}}\frac{\mathrm{d}s}{B^2}|v_\parallel|^3\left[\chi'(\nabla\psi\times\mathbf{h})\cdot\nabla\varphi - \left(2\frac{\partial B}{\partial\psi} - \frac{B}{B^\varphi}\frac{\partial B^\varphi}{\partial\psi}\right)\right]. \tag{30}$$

In contrast to Eqs. (18) and (20) in Eqs. (29) and (30), integration over φ is transformed to integration over s in the same way as in Eq. (23).

Now introducing the definition

$$\frac{d\theta}{dt} = \frac{\Delta\hat{\theta}}{\tau_b}, \tag{31}$$

as well as the new pitch-angle variable b' connected with $J_\perp$ as

$$b' = v^2/(J_\perp B_0), \tag{32}$$

where B_0 is some reference magnetic field, one finally obtains

$$\frac{d\theta}{dt} = \frac{v^2 B_0}{2\omega_{c0}}\left[\frac{\partial\hat{G}_j/\partial b'}{\partial\hat{I}_j/\partial b'} + \frac{2}{3}\frac{\partial\hat{V}_j/\partial b'}{\partial\hat{I}_j/\partial b'} + \frac{2e}{mv^2}\Phi'\right], \tag{33}$$

where $\omega_{c0}=eB_0/(mc)$ and

$$\hat{G}_j = \frac{1}{3}\int_{s_j^{\min}}^{s_j^{\max}}\frac{\mathrm{d}s}{B}\sqrt{1-\frac{B}{B_0 b'}}\left(4\frac{B_0}{B} - \frac{1}{b'}\right)\frac{1}{B_0}\frac{\partial B}{\partial\psi}, \tag{34}$$

$$\hat{V}_j = \int_{s_j^{\min}}^{s_j^{\max}}\frac{\mathrm{d}s}{B^2}\left(1-\frac{B}{B_0 b'}\right)^{3/2}\left[\chi'(\nabla\psi\times\mathbf{h})\cdot\nabla\varphi - \left(2\frac{\partial B}{\partial\psi} - \frac{B}{B^\varphi}\frac{\partial B^\varphi}{\partial\psi}\right)\right]. \tag{35}$$

With this, in Eq. (31) τ_b is used in a form obtained from Eq. (28),

$$\tau_{b,j} = \frac{4B_0 b'^2}{v}\frac{\partial\hat{I}_j}{\partial b'}, \quad \hat{I}_j = \int_{s_j^{\min}}^{s_j^{\max}}\frac{\mathrm{d}s}{B}\sqrt{1-\frac{B}{B_0 b'}}. \tag{36}$$

The velocity of the bounce averaged poloidal drift can be found now from Eq. (13) ($d\psi=0$, $d\varphi=0$), Eqs. (31) and (33) as

$$\hat{v}_{\theta,i} = |\mathbf{e}_{\theta_0,i}|\frac{d\theta}{dt}, \tag{37}$$

where i is numbering the local minima of B along the magnetic field line and $\mathbf{e}_{\theta_0,i}$ is $\mathbf{e}_{\theta_0}$ at the corresponding local minimum of B for $s=s_{\min,i}$.

Here, still an arbitrary representation of the magnetic field can be used. In particular, Eqs. (33)–(35) are also valid for magnetic fields given in Boozer magnetic coordinates. In this case χ represents the rotational transform ι and $\hat{V}_j$ [Eq. (35)] can be calculated using the equality

$$\chi'(\nabla\psi\times\mathbf{h})\cdot\nabla\varphi - \left(2\frac{\partial B}{\partial\psi} - \frac{B}{B^\varphi}\frac{\partial B^\varphi}{\partial\psi}\right) = -B\frac{F'+\iota I'}{F+\iota I}, \tag{38}$$

where $cF(\psi)/2$ and $cI(\psi)/2$ are the poloidal (external with respect to the magnetic surface) and toroidal electric currents, respectively. With this, corresponding results of Ref. 3 can be obtained [Eq. (56) of Ref. 3 has a misprint: $1/B$ before $\partial B/\partial\psi$ should be replaced by $1/B_0$].

Further on, the real-space representation of the magnetic field is used. The coordinate φ is chosen to be the geometrical toroidal angle and cylindrical coordinates ρ, φ, and z are used. In this case, Eqs. (33)–(35) are valid for $d\theta/dt$ calculations. In accordance with Eqs. (21) and (22) $\partial B/\partial\psi$ and $\partial B^\varphi/\partial\psi$ now mean the following operations:

$$\frac{\partial B}{\partial \psi}=\frac{1}{B_\varphi}\left(\frac{\partial \theta_0}{\partial \rho}+\chi'\varphi\frac{\partial \psi}{\partial \rho}\right)\frac{\partial B}{\partial z}-\frac{1}{B_\varphi}\left(\frac{\partial \theta_0}{\partial z}+\chi'\varphi\frac{\partial \psi}{\partial z}\right)\frac{\partial B}{\partial \rho}, \tag{39}$$

$$\frac{\partial B^\varphi}{\partial \psi}=\frac{1}{B_\varphi}\left(\frac{\partial \theta_0}{\partial \rho}+\chi'\varphi\frac{\partial \psi}{\partial \rho}\right)\frac{\partial B^\varphi}{\partial z}-\frac{1}{B_\varphi}\left(\frac{\partial \theta_0}{\partial z}+\chi'\varphi\frac{\partial \psi}{\partial z}\right)\frac{\partial B^\varphi}{\partial \rho}, \tag{40}$$

with $B^\varphi=B_\varphi/\rho$ in the right-hand side of Eq. (40), and B_φ being the physical φ component of $\mathbf{B}$ in cylindrical coordinates. The quantity $\hat{v}_\theta$ is calculated using Eq. (37) where

$$|\mathbf{e}_{\theta_0,i}|=\frac{1}{B_\varphi}\sqrt{\left(\frac{\partial \psi}{\partial \rho}\right)^2+\left(\frac{\partial \psi}{\partial z}\right)^2}\quad (s=s_{\min,i}), \tag{41}$$

which has been obtained from Eq. (12).

III. CALCULATION OF $\nabla\psi$ AND $\nabla\theta_0$

For a toroidal magnetic field available in real-space coordinates, calculation of $\nabla\psi$ can be done with the help of equations (see, e.g., Refs. 10 and 11)

$$\frac{dP_i}{ds}=-\frac{1}{B}\frac{\partial B^j}{\partial \xi^i}P_j, \tag{42}$$

where B^j are the contravariant components of $\mathbf{B}$ in real space coordinates ξ^i, whereas $P_j=\partial\psi/\partial\xi^j$ are the covariant components of $\mathbf{P}\equiv\nabla\psi$. From Ref. 10, it follows that Eq. (42) is a consequence of the equality $\mathbf{B}\cdot\nabla\psi=0$. Since $\mathbf{B}\cdot\nabla\theta_0=0$, analogous equations,

$$\frac{dQ_i}{ds}=-\frac{1}{B}\frac{\partial B^j}{\partial \xi^i}Q_j, \tag{43}$$

can be used for calculating the covariant vector $\mathbf{Q}\equiv\nabla\theta_0$ $(Q_j=\partial\theta_0/\partial\xi^j)$.

In this approach, the functions ψ and θ_0 represent integrals of the differential equations of the magnetic field line. It is well known that in an arbitrary toroidal magnetic field one can always find two independent integrals of the equations of the magnetic field lines (see, e.g., Ref. 12). In the case of the existence of magnetic surfaces (regular or island surfaces) one of these integrals can be found as a single valued integral, ψ, namely, the magnetic surface function. Another one (which is represented by θ_0 in our case) is not single valued and $\nabla\theta_0$ increases continuously along the magnetic field line (in the case of $d\iota/d\psi\neq 0$ where ι is the rotational transform).

In general, there exists an infinite number of integrals of the magnetic field line equations. Every such integral is a linear combination of the above mentioned two independent integrals. So, there are many not single valued integrals and only the ψ integral is single valued in case of existing magnetic surfaces.

Equation (42) [as well as Eq. (43)] together with the equations of the magnetic field line are valid for calculating the gradient of any integral of the magnetic field line equations. The quantity $\nabla\psi$ is obtained by an appropriate choice of the starting value of $\nabla\psi$, $\nabla\psi_{\rm st}$, which is the normal to the magnetic surface in the starting point of the integration. The quantity $\nabla\theta_0$ can be obtained with the help of the same differential equations but the starting value of $\nabla\theta_0$ should be different from the starting value of $\nabla\psi$. According to the Clebsch representation of $\mathbf{B}$ it can be presented, e.g., as $\nabla\theta_{0\rm st}=(\mathbf{B}\times\nabla\psi_{\rm st})/|\nabla\psi_{\rm st}|^2$.

Note that if the magnetic surface does not exist (e.g., stochastic regions, destroyed magnetic surfaces), then ψ also turns out to be one of the not single valued integrals and $\nabla\psi$ increases continuously along the magnetic field line.

IV. NORMALIZED VELOCITY OF THE POLOIDAL DRIFT, ASSESSMENT OF $J_\parallel$ CONTOURS, AND FLUX SURFACE AVERAGED QUANTITIES

To analyze the computational results it is convenient to present the quantity $\hat{v}_\theta$ in a normalized form. The value of $\hat{v}_\theta$ for a deeply trapped particle near the magnetic axis of an $l=2$ stellarator with a large aspect ratio is used for the normalization. With such a normalization, the value of $\hat{v}_\theta$ is determined as

$$\hat{v}_\theta=\frac{v^2}{\omega_{c0}}\frac{\varepsilon_h}{r}\hat{v}_{\theta,\rm norm}, \tag{44}$$

where r is the average radius of the magnetic surface and ε_h is the helical ripple of the magnetic field. According to Ref. 13, for a stellarator with a large aspect ratio $\hat{v}_\theta$ is determined as

$$\hat{v}_\theta=\frac{1}{2}l\frac{v_\perp^2\varepsilon_h}{\omega_c r}\left[\frac{2E(\kappa^2)}{K(\kappa^2)}-1\right], \tag{45}$$

with $K(\kappa^2)$ and $E(\kappa^2)$ being the complete elliptic integrals of the first and the second kind, respectively, $[\kappa^2=v_{\|0}^2/(2\varepsilon_h v^2)]$. So, for the $l=2$ conventional stellarator $\hat{v}_{\theta,l2,\rm norm}$ is determined as

$$\hat{v}_{\theta,l2,\rm norm}=\frac{2E(\kappa^2)}{K(\kappa^2)}-1. \tag{46}$$

In the general case it follows from Eqs. (44), (37), and (33) that

$$\hat{v}_{\theta,\rm norm}=\frac{1}{2}\frac{r}{\varepsilon_h}B_0|\mathbf{e}_{\theta_0,i}|\times\left(\frac{\partial \hat{G}_j/\partial b'}{\partial \hat{I}_j/\partial b'}+\frac{2}{3}\frac{\partial \hat{V}_j/\partial b'}{\partial \hat{I}_j/\partial b'}+\frac{2e}{mv^2}\Phi'\right). \tag{47}$$

A numerical analysis of $\hat{v}_\theta$ Eq. (44), as well as of the radial bounce-averaged trapped particle drift $v_{\rm an}$ allows for a convenient assessment of $J_\parallel$ contours in the vicinity of a magnetic surface under consideration. This is realized by an assessment of the angle $\gamma_{J_\parallel}$ between the $J_\parallel$ contour and the magnetic surface cross section. In accordance with Refs. 3 and 14,

$$v_{{\rm an},i}=\frac{\delta\psi}{\tau_b|\nabla\psi_i|}=\frac{v^2}{2\omega_{c0}}\frac{1}{|\nabla\psi_i|}\frac{\partial g_j/\partial b'}{\partial \hat{I}_j/\partial b'}, \tag{48}$$

where

$$g_j = \frac{1}{3}\int_{s_j^{\min}}^{s_j^{\max}} \frac{\mathrm{d}s}{B}\sqrt{1-\frac{B}{B_0 b'}}\left(4\frac{B_0}{B}-\frac{1}{b'}\right)|\nabla\psi|k_G, \tag{49}$$

k_G is the geodesic curvature of the magnetic field line, and $\nabla\psi_i$ is $\nabla\psi$ at the ith local minimum of B along the magnetic field line. Using Eqs. (37), (33), and (48) one obtains

$$\gamma_{J_\parallel} = \arctan\frac{v_{\mathrm{an},i}}{\hat{v}_{\theta,i}}, \quad \gamma_c = \frac{2}{\pi}\gamma_{J_\parallel}, \tag{50}$$

with

$$\frac{v_{\mathrm{an},i}}{\hat{v}_{\theta,i}} = \frac{1}{|\nabla\psi_i|}\frac{\partial g_j/\partial b'}{\partial \hat{I}_j/\partial b'} \times\left[B_0|\mathbf{e}_{\theta_0,i}|\left(\frac{\partial \hat{G}_j/\partial b'}{\partial \hat{I}_j/\partial b'}+\frac{2}{3}\frac{\partial \hat{V}_j/\partial b'}{\partial \hat{I}_j/\partial b'}+\frac{2e}{mv^2}\Phi'\right)\right]^{-1}. \tag{51}$$

In the calculations, $|\gamma_c|$ can be realized within the limits $[0,1]$. For $|\gamma_c|=1$ the $J_\parallel$ contour is perpendicular to the magnetic surface and most probably such a contour is not closed. For small $|\gamma_c|$ the angle between the $J_\parallel$ contour and the magnetic surface is small and one can expect that the corresponding $J_\parallel$ contour is closed and is closely tied to the magnetic surface.

Equations (37), (33), and (50) characterize the poloidal drift in every local minimum of B. Now these equations are employed to obtain flux surface averaged quantities which characterize in total the poloidal drift as well as combined poloidal and radial drifts. These quantities denoted further as Γ_{wp} and Γ_c correspond to integral effects for $\hat{v}_\theta^2$ and γ_c^2 obtained by an appropriate average of $\hat{v}_\theta^2$ and γ_c^2 over a magnetic surface and over pitch angles. Averaging over a magnetic surface is performed by the rule

$$\langle A\rangle = \lim_{L\to\infty}\left(\int_0^L \frac{\mathrm{d}s}{B}\right)^{-1}\int_0^L \mathrm{d}s\frac{A}{B}. \tag{52}$$

In fact such a rule corresponds to averaging over a thin layer between neighboring magnetic surfaces.[11]

Integrating the quantities $\hat{v}_\theta^2$ and γ_c^2 over the phase-space volume and averaging over a magnetic surface using the rule (52) gives

$$F_{wp}^* = \left\langle\int \hat{v}_\theta^2 f d\Gamma_{w,J_\perp}\right\rangle, \tag{53}$$

$$F_c^* = \left\langle\int \gamma_c^2 f d\Gamma_{w,J_\perp}\right\rangle, \tag{54}$$

where $f=f(w,\psi)$ is the distribution of trapped particles and $d\Gamma_{w,J_\perp}$ is the phase space volume element

$$d\Gamma_{w,J_\perp} = \sum_{\sigma=\pm1}\frac{\pi B}{mv_\parallel}dJ_\perp dw = \frac{2\pi B}{m|v_\parallel|}dJ_\perp dw. \tag{55}$$

From Eqs. (53)–(55) it follows

$$F_{wp}^* = \left\langle\int_{e\Phi}^\infty \mathrm{d}w\int_{J_{\perp\min}}^{J_{\perp\max}}\mathrm{d}J_\perp\frac{2\pi B}{m|v_\parallel|}f\hat{v}_\theta^2\right\rangle, \tag{56}$$

$$F_c^* = \left\langle\int_{e\Phi}^\infty \mathrm{d}w\int_{J_{\perp\min}}^{J_{\perp\max}}\mathrm{d}J_\perp\frac{2\pi B}{m|v_\parallel|}f\gamma_c^2\right\rangle, \tag{57}$$

with $J_{\perp\min}=v^2/B_{\max}^{\mathrm{abs}}$ and $J_{\perp\max}=v^2/B$.

Equations (56) and (57) are further modified for the description of collisionless α-particle confinement. Here, the influence of an ambipolar radial electric field is neglected because of the large α-particle energy. Under such a condition, after substituting Eqs. (37), (33), and (50) into Eqs. (56) and (57), changing the order of integration over $J_\perp$ and s, and changing the integration over $J_\perp$ to an integration over b' with the help of Eq. (32), one obtains the following expressions:

$$F_{wp}^* = \frac{\sqrt{2}}{m}\frac{1}{R_0^2\omega_{c0}^2}\Gamma_{wp}\int_{e\Phi}^\infty \mathrm{d}wv^5 f, \tag{58}$$

$$F_c^* = \frac{8\sqrt{2}}{m}\Gamma_c\int_{e\Phi}^\infty \mathrm{d}wvf, \tag{59}$$

with Γ_{wp} and Γ_c being defined as

$$\Gamma_{wp} = \frac{\pi R_0^2}{\sqrt{2}}\lim_{L_s\to\infty}\left(\int_0^{L_s}\frac{ds}{B}\right)^{-1}B_0^2\langle|\mathbf{e}_{\theta_0}|\rangle^2 \times\int_{B_{\min}^{\mathrm{abs}}/B_0}^{B_{\max}^{\mathrm{abs}}/B_0}\mathrm{d}b'\sum_{j=1}^{j_{\max}}\left(\frac{\partial \hat{G}_j^*}{\partial b'}\right)^2\left(\frac{\partial \hat{I}_j}{\partial b'}\right)^{-1} \tag{60}$$

and

$$\Gamma_c = \frac{\pi}{2\sqrt{2}}\lim_{L_s\to\infty}\left(\int_0^{L_s}\frac{ds}{B}\right)^{-1}\times\int_{B_{\min}^{\mathrm{abs}}/B_0}^{B_{\max}^{\mathrm{abs}}/B_0}\mathrm{d}b'\sum_{j=1}^{j_{\max}}\gamma_{cj}^2\frac{\partial \hat{I}_j}{\partial b'}. \tag{61}$$

Here, R_0 is the major radius of the torus and $B_{\min}^{\mathrm{abs}}$ and $B_{\max}^{\mathrm{abs}}$ are the absolute minimum and maximum of B within a sufficiently large interval $[0,L_s]$, respectively. The index j numbers the field line intervals $[s_j^{\min},s_j^{\max}]$ where $b'-B/B_0\geq 0$ for a given $J_\perp$ and w. The derivative $\partial\hat{G}_j^*/\partial b'$ in Eq. (60) has the meaning

$$\frac{\partial \hat{G}_j^*}{\partial b'} = \frac{\partial \hat{G}_j}{\partial b'}+\frac{2}{3}\frac{\partial \hat{V}_j}{\partial b'}. \tag{62}$$

It is of interest to obtain the maximum of the parameter Γ_c, Γ_{cm}, for the hypothetically most unfavorable conditions corresponding to $|\gamma_{c,j}|=1$ for all trapped particles. In such a case, it is convenient to perform the integration over $J_\perp$ before the integration over s in Eq. (57) for $\gamma_c^2=1$. As a result one obtains

$$F_{cm}^* = \frac{4\pi}{m}\left\langle\sqrt{1-\frac{B}{B_{\max}^{\mathrm{abs}}}}\right\rangle\int_{e\Phi}^\infty \mathrm{d}wvf. \tag{63}$$

From Eqs. (63) and (59), it follows that

$$\Gamma_{cm} = \frac{\pi}{2\sqrt{2}} \left\langle \sqrt{1 - \frac{B}{B_{\max}^{\text{abs}}}} \right\rangle. \tag{64}$$

Note that Eq. (63) gives in fact the phase volume occupied by trapped particles averaged with the weight f using the rule (52). For the model of a classical stellarator with a sufficiently large aspect ratio

$$\Gamma_{cm}^{\text{cl}} = \sqrt{\varepsilon_h}, \quad \Gamma_{wp}^{\text{cl}} \approx (l\varepsilon_h R_0/r)^2 \sqrt{\varepsilon_h}. \tag{65}$$

Such an estimation of Γ_{wp}^{cl} can be obtained using Eq. (45).

As in Ref. 3, a monoenergetic distribution function,

$$f = n \frac{m^{3/2}}{4\sqrt{2}\pi\sqrt{E - e\Phi}} \delta(w - E), \tag{66}$$

is used for calculation of the integrals over w. With this one obtains

$$\int_{e\Phi}^{\infty} \mathrm{d}w v f = \frac{mn}{4\pi}, \quad \int_{e\Phi}^{\infty} \mathrm{d}w v^5 f = \frac{mn}{4\pi} v^4, \tag{67}$$

with $v^2 = 2(E - e\Phi)/m$. With such a definition, Eqs. (58) and (59) result in the final form,

$$F_{wp}^* = \frac{\sqrt{2}}{4\pi} \Gamma_{wp} \frac{v^2 \rho_L^2}{R_0^2} n, \tag{68}$$

$$F_c^* = \frac{2\sqrt{2}}{\pi} \Gamma_c n, \tag{69}$$

with $\rho_L = v/\omega_{c0}$ being the characteristic Larmor radius.

The parameters Γ_{wp} and Γ_c [Eqs. (60) and (61)] which characterize confinement properties of a magnetic configuration can be computed efficiently in a field line tracing code.

In conclusion of this section some remarks are necessary. (i) When computing Γ_{wp} instead of $|\mathbf{e}_{\theta_0,i}|$ an averaged value $\langle |\mathbf{e}_{\theta_0}| \rangle$ is used. This is in contrast to the computation of Γ_c where $|\mathbf{e}_{\theta_0,i}|$ is used. The choice of $\langle |\mathbf{e}_{\theta_0}| \rangle$ in the computation of Γ_{wp} gives a higher weight to $d\theta/dt$ compared to $\hat{v}_\theta$. (ii) It follows from explanation after Eq. (51) that values of $|\gamma_c|$ close to unity are more unfavorable for the confinement properties of a magnetic configuration. To manifest more strongly the role of larger values of $|\gamma_c|$ in Γ_c, the quantities $\gamma_{c,j}^2$ are used in Eqs. (57) and (61) (instead of $|\gamma_{c,j}|$). (iii) In the case of particles being trapped within several neighboring magnetic ripples, $|\mathbf{e}_{\theta_0,i}|$ is taken from the most deep ripple within the jth segment of the field line. (iv) When comparing the role of Γ_{wp} and Γ_c in an optimization problem one should bear in mind the following. In principle, an increase of Γ_{wp} and a decrease of Γ_c correspond to an optimization procedure. At the same time, in such a procedure it is important to recognize the presence of trapped particles with a small poloidal drift velocity. Those are the most unfavorable ones with respect to confinement properties of a device. However, the role of such particles can be hidden in Γ_{wp} because of the presence of trapped particles with large poloidal drift velocities. In contrast, Γ_c is most sensitive to the existence of trapped particles with small poloidal drift. So, although both parameters, Γ_{wp} and Γ_c, are of interest, an analysis of the parameter Γ_c is most important for an optimization problem.

V. COMPUTATIONAL RESULTS

The possibilities of the proposed technique are further demonstrated by its application to four stellarator-type magnetic configurations. These configurations are (i) the standard vacuum CHS configuration, (ii) the drift-orbit optimized (inward shifted) CHS[6] configuration, (iii) a vacuum configuration of U-2M,[7] as well as (iv) a W7-X[1] configuration with finite beta, $\beta \approx 2\%$, where an equilibrium computed by the HINT2[5] code is used. In the following numerical computations the radial electric field is assumed to be zero, $\Phi' = 0$. This is fully justified, because the radial electric field has a negligible effect on α-particle confinement.

The CHS configuration is characteristic for a small aspect ratio, A_p ($A_p = R/a$), $l=2$ heliotron-torsatron device. It is characterized by $A_p \approx 5$, $n_p = 8$, and $0.3 \leq \iota \leq 1.0$. In contrast to the standard CHS configuration, the drift-orbit-optimized CHS configuration is an inward shifted configuration. Its properties are rather close to those for σ-optimization.[16] The U-2M device is an $l=2$ torsatron with $A_p \approx 8$, $n_p = 4$ with an additional toroidal magnetic field. The W7-X stellarator is an optimized stellarator utilizing modular coils and is now under construction at Greifswald, Germany.

Computations of **B** for CHS and W7-X are performed in the same way as in Refs. 15 and 17, where a study of the effective ripple had been carried out. For the **B** computation of U-2M the code of Ref. 18 is used. Here, the influence of current-feeds and detachable joints of the helical winding is neglected. For CHS and U-2M **B** is computed using the Biot–Savart law based on the data base for helical windings and additional coils of the devices. The HINT2 output for **B** presented in real-space coordinates (ρ, φ, z) is used for the calculations of W7-X. This output is given on a three-dimensional set of discrete mesh points. Between these points the **B** components are computed using three-dimensional cubic splines.

For any magnetic surface to be analyzed, the value χ' has to be computed as a first step of the computation of the poloidal motion of trapped particles. To illustrate the computation of χ', Fig. 1 shows the behavior of $\nabla\theta_0 \cdot \nabla\psi/(\varphi|\nabla\psi|^2)$ [see Eq. (7)] along the magnetic field line for one of the magnetic surfaces of the CHS standard configuration. It can be clearly seen how this quantity is oscillating with decreasing amplitude and how it approaches the final value of χ'. The plot covers 125 field periods each computed with 1280 integration steps.

Once χ' has been computed, $v_{\theta,\text{norm}}$ Eq. (47) and γ_c Eq. (50) can be calculated with the help of the relevant expressions from Sec. II. The computational results for the four magnetic configurations described above are presented in Figs. 2–5. Every figure shows results for one appropriate magnetic surface of the pertinent configuration. At the top of every figure a plot of the distribution of B/B_0 along the magnetic field line is shown. The local minima of B are marked in accordance with their numbering along the magnetic field line. The mean radius of the magnetic surface is indicated on the plot. Below the B/B_0 plot the corresponding results for $v_{\theta,\text{norm}}$ and γ_c are presented as functions of the pitch γ for a number of local minima of B. The γ parameter is defined as

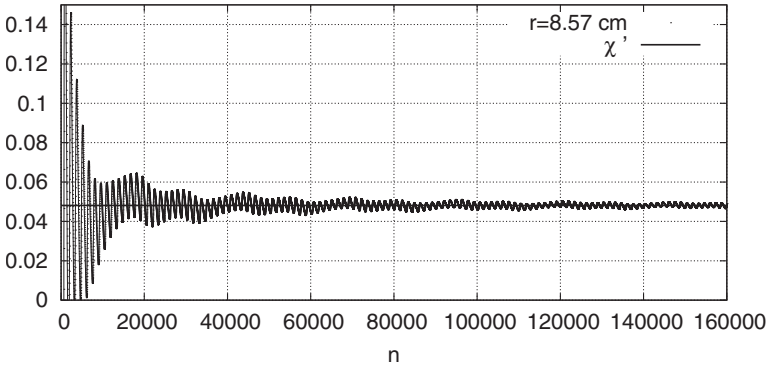

FIG. 1. Determination of χ' for the standard configuration of CHS for a magnetic surface with a moderate distance from the magnetic axis; n is the number of integration steps along the field line with 1280 steps per magnetic field period.

$\gamma = v_{\parallel 0}/v_{\perp 0}$, where $v_{\parallel 0}$ is $v_\parallel$ at a local minimum of B and $v_{\perp 0} = \sqrt{J_\perp B_0}$. The curves are marked in accordance with the numbers of the minima of B in the distribution of B/B_0 along the magnetic field line.

The results for the standard configuration of CHS are presented in Fig. 2. It can be seen from the figure that minima exist (e.g., number 25) where the functional behavior of $v_{\theta,\mathrm{norm}}$ is close to the behavior of an ideal $l=2$ heliotron-torsatron for which $v_{\theta,\mathrm{norm}}$ approaches unity at $\gamma \approx 0$, see Eq. (46). For magnetic field ripples being located towards the absolute minimum the pertinent curves are shifted to higher values and also show the influence of trapping within more than one field period at higher values of γ. For ripples approaching the absolute maximum the curves are shifted to lower values and therefore start crossing zero at smaller values. For those values of γ where $v_{\theta,\mathrm{norm}}=0$, $|\gamma_c|$ is close to unity indicating contours of $J_\parallel$ which are not closed poloidally.

Analogous results for a magnetic surface of the drift-orbit-optimized CHS configuration are shown in Fig. 3 where the distribution of B/B_0 along the magnetic field line shows the characteristic look of σ-optimization (full σ-optimization would mean that all minima have exactly the same value). One can also see that the fraction of trapped particles with v_θ values close to zero (and $|\gamma_c|$ close to unity) is much smaller than that for the standard configuration which is a clear result of the optimization.

Figure 4 presents the computational results for U-2M for device parameters of practical interest where the magnetic configuration is well centered with respect to the vacuum chamber and the rotational transform, ι, is larger than 1/3 near the magnetic axis and smaller than 1/2 at the outer surfaces ($k_\varphi = 0.31$, see in Refs. 20 and 21). Here, a magnetic surface rather close to the vacuum chamber is chosen as an example. The presence of additional toroidal field coils is a peculiarity of the U-2M device. These coils cause additional local ripples in the distribution of B along the magnetic field line and an increased number of local minima of B around the torus as it can be seen from the B/B_0 distribution in Fig. 4. For a rather big fraction of trapped particles one finds $|\gamma_c|$ values close to unity which clearly shows the unfavorable situation of the well centered magnetic configuration (see Ref. 20) which could also be improved by an inward shift of the configuration.

In Fig. 5, computational results for a magnetic surface of W7-X not far from the plasma boundary are presented. One can see that these results correlate well with the analogous results obtained in Ref. 19 for the magnetic field given in magnetic coordinates. It can also be seen in Fig. 5 that $|\gamma_c|$ values exist close to unity for a rather big fraction of minima of B but the γ intervals corresponding to such values of $|\gamma_c|$ are smaller than for U-2M indicating that a smaller number of trapped particles in each minimum is affected.

Many plots in Figs. 2–5 show curves with rather abrupt changes in $v_{\theta,\mathrm{norm}}$ and γ_c with increasing γ. These sharp changes are connected with transitions from particles being trapped within one magnetic field ripple to particles being trapped within two or more ripples.

Finally, for all four configurations in Fig. 6 radial profiles are presented for Γ_{wp}, Γ_c and Γ_{cm} calculated with the help of expressions (60), (61), and (64) from Sec. IV. Of course, for all configurations Γ_c is essentially smaller than Γ_{cm}. It follows from the presented plots that in major parts of the confinement regions, Γ_c for the inward shifted CHS configuration is essentially smaller than for the standard CHS configuration whereas Γ_{wp} for these configurations does not differ strongly. This demonstrates the larger sensitiveness of the parameter Γ_c than Γ_{wp} to improvement (or worsening) of the confinement properties of stellarator devices. For W7-X, U-2M and the standard CHS configuration Γ_c is of the same order in magnitude in the central part of the magnetic configurations, although for W7-X it is slightly smaller. For the comparison in Fig. 6 analogous results are presented (curves QI) also for the quasi-isodynamical (QI) configuration[22] optimized with respect to collisionless particle confinement with subsequent optimization towards poloidal closure of the $J_\parallel$ contours. The computations for QI are performed in magnetic coordinates. Here, results are shown for the second QI configuration in Ref. 3 where $d\theta/dt$ has been analyzed for the magnetic surface with $r/a=0.718$. It follows from the comparison that Γ_{cm} for the QI configuration has the highest value because the fraction of trapped particles in this configuration is the largest. Nevertheless, Γ_c for a major part of the confinement region for this configuration is essentially smaller than for the other configurations. This correlates with the optimization properties of this configuration. There exist a gap to the best real space configuration analyzed here (inward shifted CHS) where the closure of $J_\parallel$ contours was not a design criterion. The parameter Γ_{wp} correlates well with

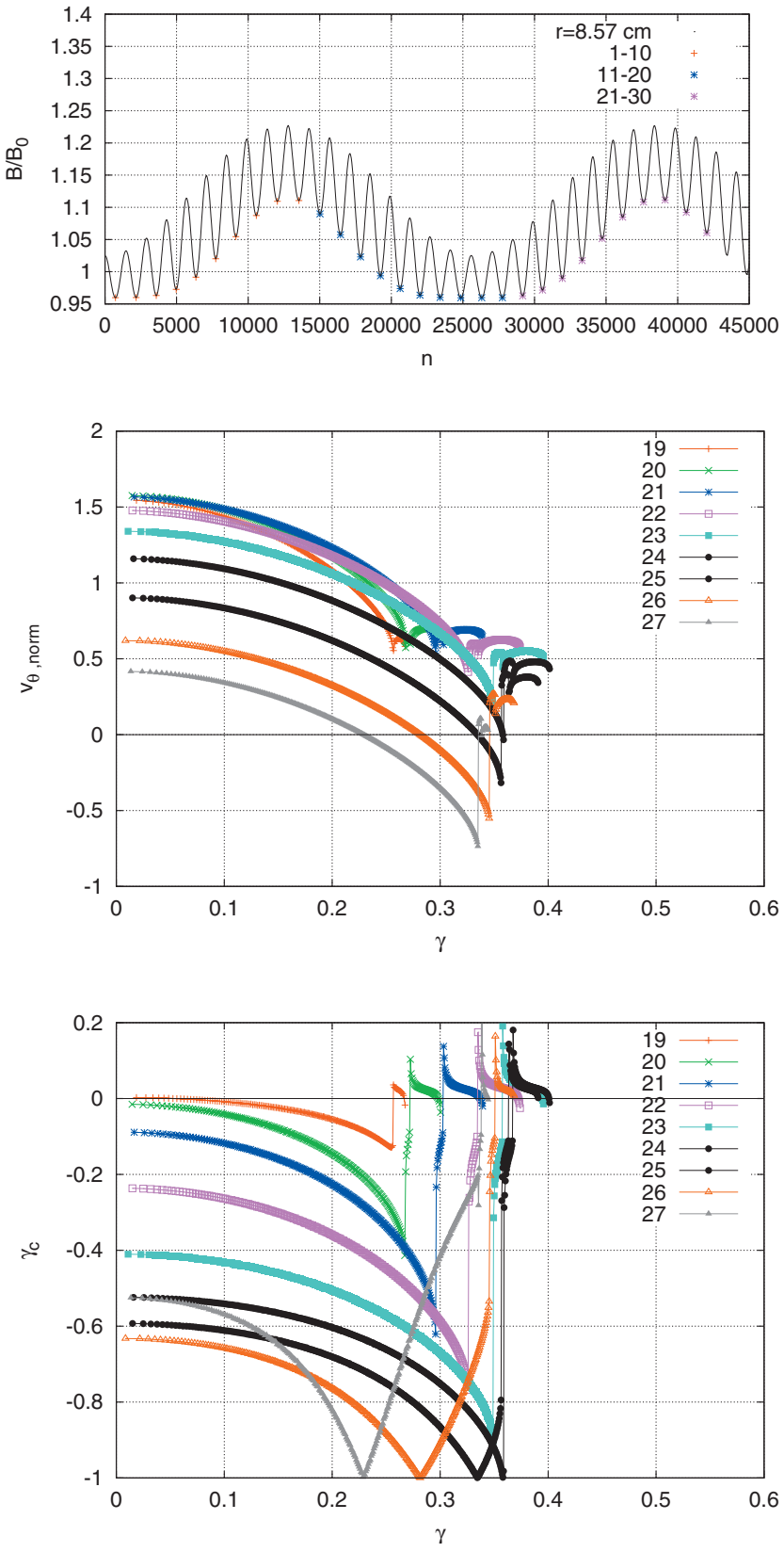

FIG. 2. (Color) Computational results for a magnetic surface of the standard CHS vacuum configuration: (top) distribution of B/B_0 along the magnetic field line, n is the number of integration steps along the field line with 1280 steps per magnetic field period; (middle) $v_{\theta,\mathrm{norm}}$ as a function of pitch-angle γ for local minima of B as indicated in the figure; (bottom) parameter γ_c as a function of pitch-angle γ for the same local minima of B.

formula (65) since ε_h is larger for CHS and QI than for U-2M and W7-X.

Overall one can see that the different choices and/or optimization strategies reflect themselves in the quite different functional dependence of $v_{\theta,\mathrm{norm}}$ and γ_c. This limited survey of configurations clearly shows the beneficial effect of inward shift (σ-optimization) also on $v_{\theta,\mathrm{norm}}$ and γ_c and not only on $\varepsilon_{\mathrm{eff}}$.

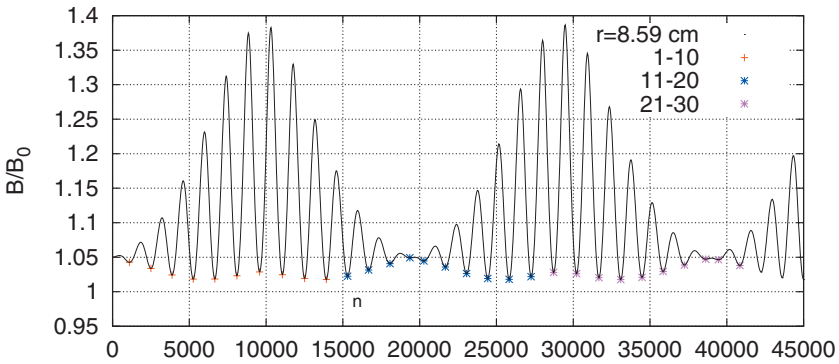

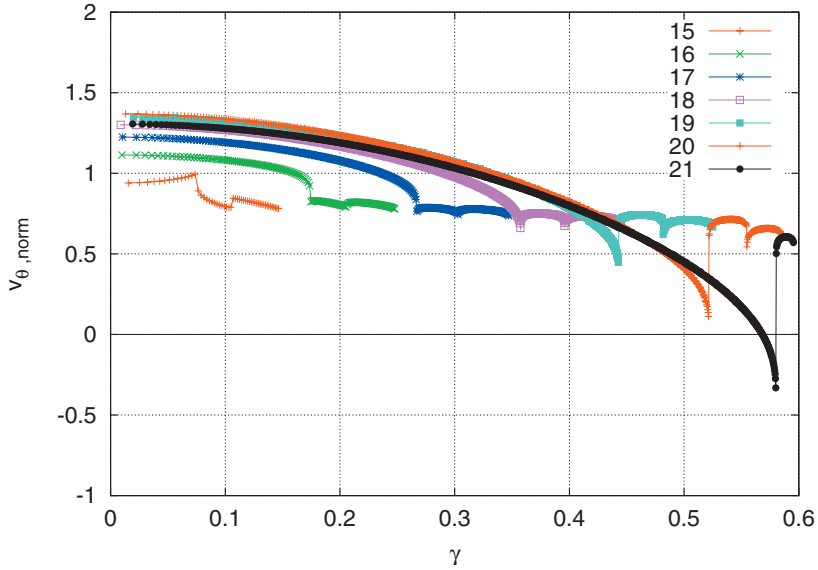

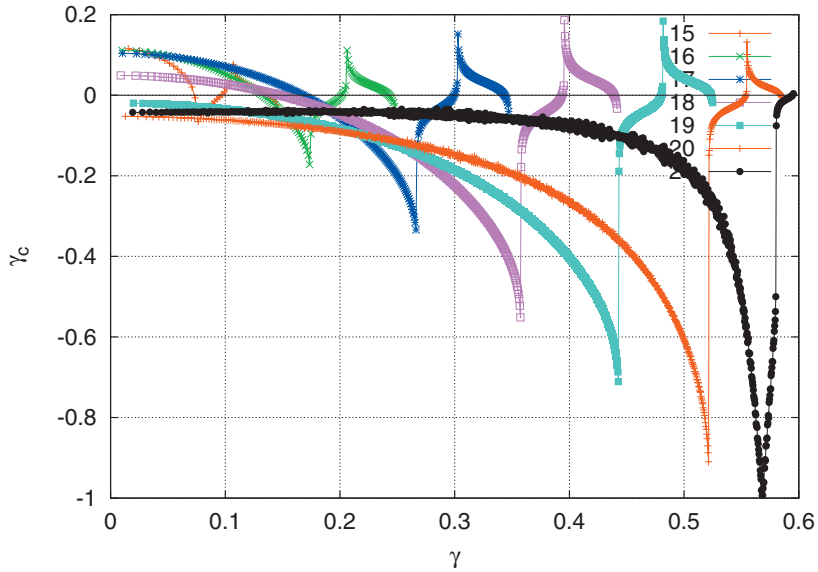

FIG. 3. (Color) Same as Fig. 2 for a magnetic surface of the drift-orbit optimized CHS configuration.

VI. CONCLUSION

This paper presents an approach to compute the bounce averaged poloidal drift velocity of trapped particles which are valid for particles being trapped within one magnetic field ripple as well as for particles being trapped within several neighboring ripples. The obtained formulas can be evaluated using a field line following code. The method is not restricted to magnetic coordinates and can directly use stellarator fields given in real-space coordinates without prior transformation to magnetic coordinates. This opens the way for direct usage of output from the equilibrium code HINT2 which is demonstrated in one of the examples. Technically,

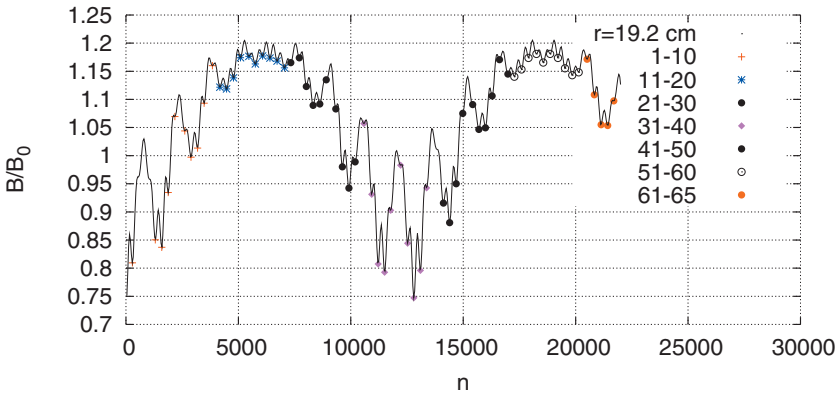

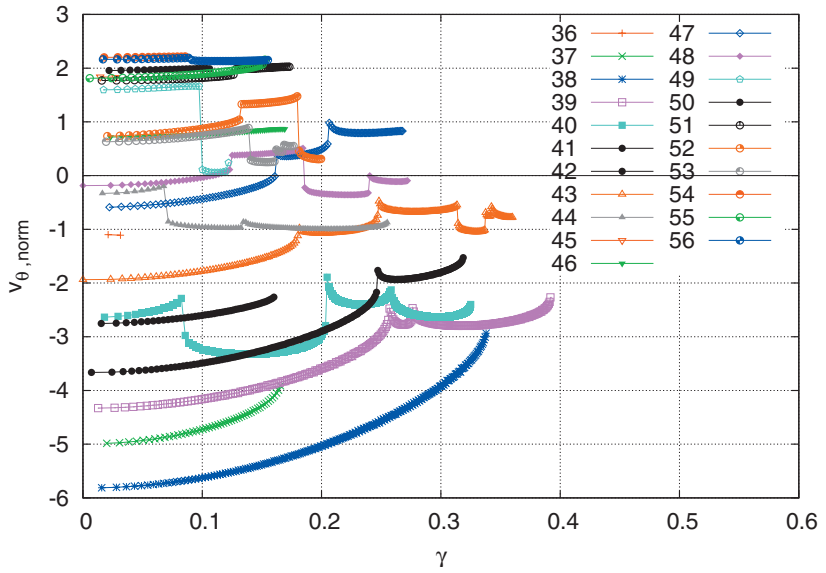

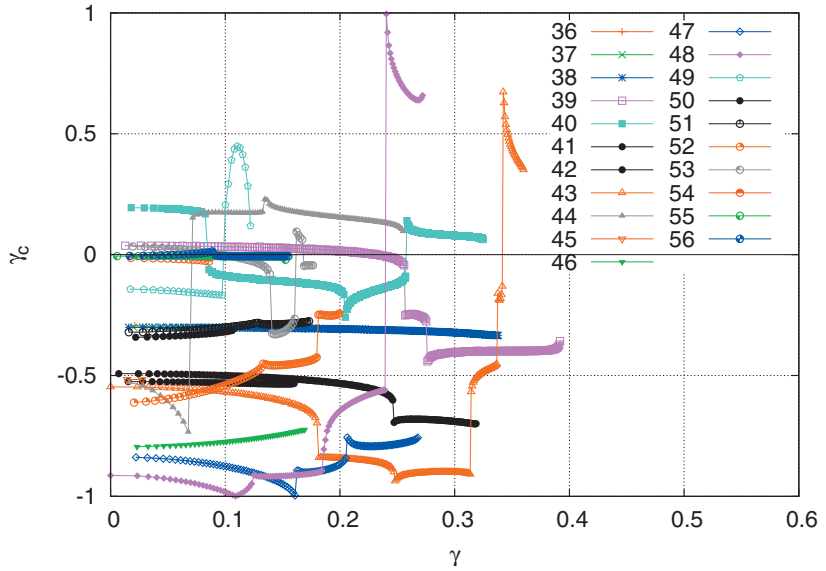

FIG. 4. (Color) Same as Fig. 2 for a magnetic surface of the U-2M configuration (the magnetic surface is close to the vacuum chamber).

one of the key points of the approach is a transformation in real-space coordinates of the multivalued poloidal variable which enters into the Clebsch representation of the magnetic field to a new poloidal variable with a single valued gradient of this quantity. This allows for simultaneous computations for a variety of trapped particles distributed along the magnetic field line which makes the numerical computation very efficient.

Among appropriate criteria for improving particle confinement in stellarators, an important role belongs to the closure of contours of $J_{\parallel}$ (see, e.g., Ref. 2). Combining studies of the radial drift as well as the poloidal drift one can con-

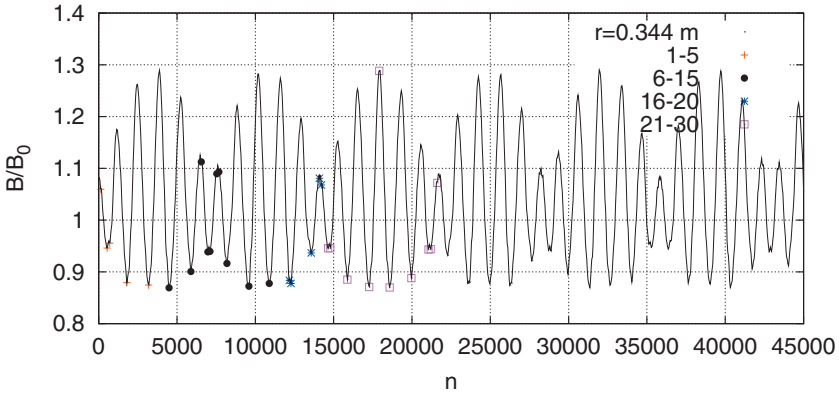

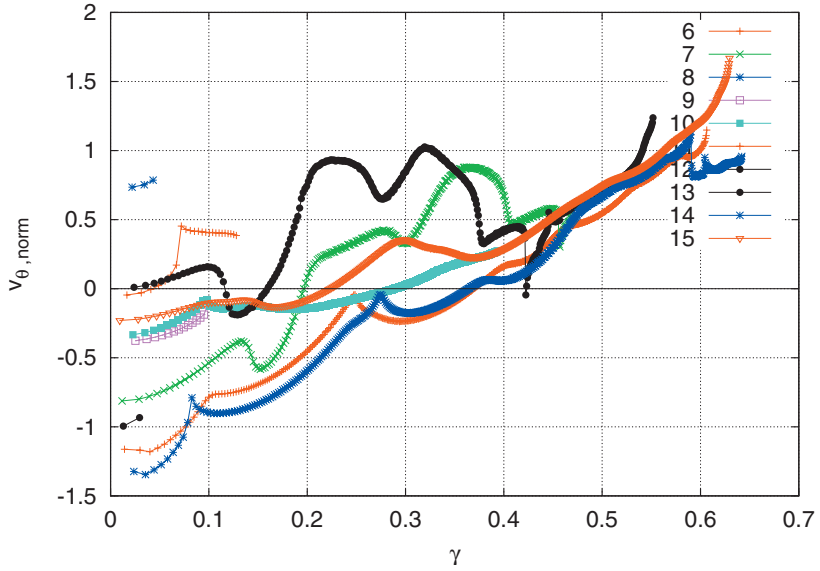

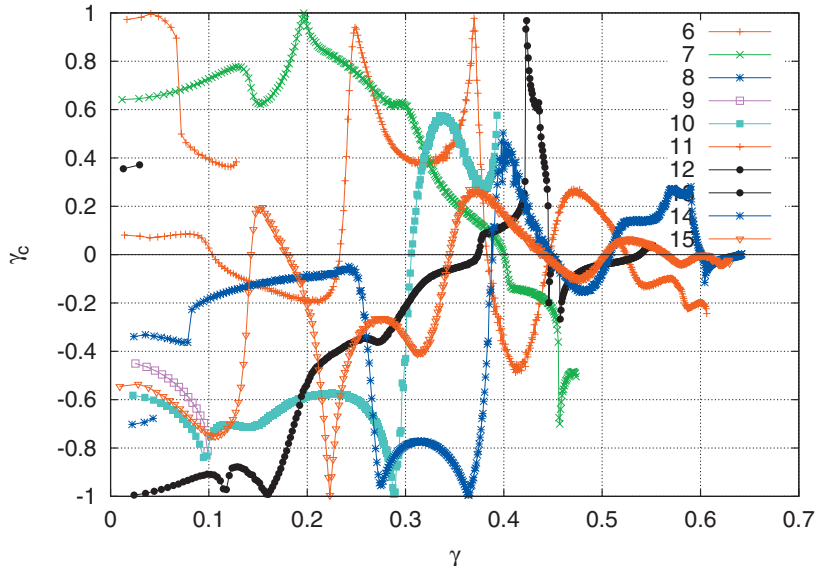

FIG. 5. (Color) Same as Fig. 2 for a magnetic surface of the W7-X configuration (the magnetic surface is not far from the plasma boundary).

veniently assess the character of $J_\parallel$ contours in the neighborhood of a magnetic surface. Small values of the parameters $\gamma_{J\parallel}$ or γ_c given in formula (50) indicate poloidally closed contours of $J_\parallel$ which are closely tied to the magnetic surface, whereas $|\gamma_c|$ values close to unity definitely indicate the presence of unclosed contours of $J_\parallel$.

With the help of equations for poloidal motion and the quantity γ_c, the flux surface averaged parameters Γ_{wp} and Γ_c [Eqs. (60) and (61)] are obtained. Both these parameters are calculated using a field line tracing code and can be used as additional targets for stellarator optimization.

To illustrate the approach, computations for four stellar-

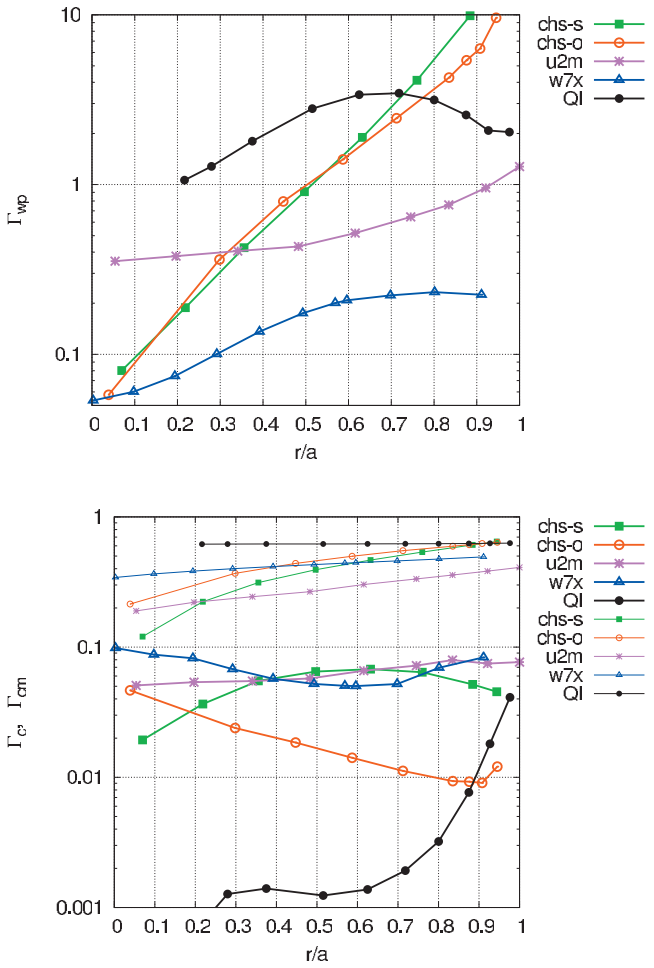

FIG. 6. (Color) Parameters Γ_{wp}, Γ_c, and Γ_{cm} as functions of r/a for specified magnetic configurations. Thick lines are used for Γ_{wp} (upper plot) and Γ_c (lower plot), whereas thin lines are used for Γ_{cm}. (chs-s): standard CHS configuration; (chs-o): optimized CHS configuration (inward shifted); (u2m): U-2M; (w7x): W7-X; (QI): quasi-isodynamical configuration; r is the mean radius of a given magnetic surface, a is the mean radius of the outermost magnetic surface. The results of Figs. 2–5 correspond to r/a =0.497, 0.587, 0.92, and 0.8, respectively.

ator configurations with quite different results are shown. In one of the examples, the drift-orbit optimized CHS configuration (inward shifted configuration), one can see the beneficial effect of σ-optimization on the bounce averaged poloidal drift velocity and the pertinent closure of contours of $J_{\|}$.

The theoretical as well as the numerical approach presented here very well complement the effective ripple as target quantity for optimization by putting more significance to fast particle confinement which is not covered well by the effective ripple.

ACKNOWLEDGMENTS

The authors would like to thank Dr. M. Isobe, Professor K. Matsuoka, and Professor S. Okamura (NIFS, Japan) for providing the CHS coil data. The authors are indebted to Dr. Y. Suzuki (NIFS, Japan) for providing HINT2 data for the magnetic field of W7-X.

This work, supported by the European Communities under the Contract of Association between EURATOM and the Austrian Academy of Sciences, was carried out within the framework of the European Fusion Development Agreement. The views and opinions expressed herein do not necessarily reflect those of the European Commission. Additional funding is provided by the Austrian Science Foundation, FWF, under Contract No. P16797-N08.

[1] G. Grieger, W. Lotz, P. Merkel, J. Nührenberg, J. Sapper, E. Strumberger, H. Wobig, the W7-X Team, R. Burhenn, V. Erckmann, U. Gasparino, L. Giannone, H. J. Hartfuss, R. Jaenicke, G. Kühner, H. Ringler, A. Weller, F. Wagner, and the W7-AS Team, Phys. Fluids B **4**, 2081 (1992).
[2] M. I. Mikhailov, V. D. Shafranov, A. A. Subbotin, M. Yu. Isaev, J. Nührenberg, R. Zille, and W. A. Cooper, Nucl. Fusion **42**, L23 (2002).
[3] V. V. Nemov, S. V. Kasilov, W. Kernbichler, and G. O. Leitold, Phys. Plasmas **12**, 112507 (2005).
[4] A. H. Reiman and H. S. Greenside, J. Comput. Phys. **75**, 423 (1988).
[5] Y. Suzuki, N. Nakajima, K. Watanabe, Y. Nakamura, and T. Hayashi, Nucl. Fusion **46**, L19 (2006).
[6] S. Okamura, K. Matsuoka, R. Akiyama, D. S. Darrow, A. Ejiri, A. Fujisawa, M. Fujiwara, M. Goto, K. Ida, H. Idei, H. Iguchi, N. Inoue, M. Isobe, K. Itoh, S. Kado, K. Khlopenkov, T. Kondo, S. Kubo, A. Lazaros, S. Lee, G. Matsunaga, T. Minami, S. Morita, S. Murakami, N. Nakajima, N. Nikai, S. Nishimura, I. Nomura, S. Ohdachi, K. Ohkuni, M. Osakabe, R. Pavlichenko, B. J. Peterson, R. Sakamoto, H. Sanuki, M. Sasao, A. Shimizu, Y. Shirai, S. Sudo, S. Takagi, C. Takahashi, S. Takayama, M. Takechi, K. Tanaka, K. Toi, T. Watari, K. Yamazaki, M. Yokoyama, and Y. Yoshimura, Nucl. Fusion **39**, 1337 (1999).
[7] O. S. Pavlichenko and the U-2M group, Plasma Phys. Controlled Fusion **35**, B223 (1993).
[8] A. I. Morozov and L. S. Solov'ev, in *Reviews of Plasma Physics*, edited by M. A. Leontovich (Consultants Bureau, New York, 1966), Vol. 2, p. 201; see also *Voprosy Teorii Plazmy* (Atomizdat, Moscow, 1963), Vol. 2, p. 177 (in Russian).
[9] A. H. Boozer, Phys. Fluids **24**, 1999 (1981).
[10] V. V. Nemov, Nucl. Fusion **28**, 1727 (1988).
[11] V. V. Nemov, S. V. Kasilov, W. Kernbichler, and M. F. Heyn, Phys. Plasmas **6**, 4622 (1999).
[12] A. I. Morozov and L. S. Solov'ev, in *Reviews of Plasma Physics*, edited by M. A. Leontovich (Consultants Bureau, New York, 1966), Vol. 2, p. 3; see also *Voprosy Teorii Plazmy* (Atomizdat, Moscow, 1963), Vol. 2, p. 3 (in Russian).
[13] A. A. Galeev and R. Z. Sagdeev, in *Reviews of Plasma Physics*, edited by M. A. Leontovich (Consultants Bureau, New York, 1979), Vol. 7, p. 257; see also *Voprosy Teorii Plazmy* (Atomizdat, Moscow, 1963), Vol. 2, p. 205 (in Russian).
[14] V. V. Nemov, Phys. Plasmas **6**, 122 (1999).
[15] M. F. Heyn, M. Isobe, S. V. Kasilov, W. Kernbichler, K. Matsuoka, V. V. Nemov, S. Okamura, and O. S. Pavlichenko, Plasma Phys. Controlled Fusion **43**, 1311 (2001).
[16] H. E. Mynick, Phys. Fluids **26**, 1008 (1983).
[17] V. V. Nemov, S. V. Kasilov, W. Kernbichler, B. Seiwald, Y. Suzuki, and J. Geiger, in *34th EPS Conference on Plasma Physics, Warsaw, Poland, 2–6 July 2007*, edited by P. Gasior and J. Wolowski (European Physical Society, Mulhouse, 2007), ECA Vol. 31F, P–4.063.
[18] V. V. Nemov, V. N. Kalyuzhnyj, S. V. Kasilov, W. Kernbichler, G. G. Lesnyakov, B. Seiwald, and N. T. Besedin, in *34th EPS Conference on Plasma Physics, Warsaw, Poland, 2–6 July 2007*, edited by P. Gasior and J. Wolowski (European Physical Society, Mulhouse, 2007), ECA Vol. 31F, P–1.077.
[19] V. V. Nemov, W. Kernbichler, S. V. Kasilov, G. O. Leitold, and L. P. Ku, in *33rd EPS Conference on Plasma Physics, Rome, Italy, 19–23 June 2006*, edited by F. De Marco and G. Vlad (European Physical Society, Mulhouse, 2006), ECA Vol. 30I, P–4.164.
[20] B. Seiwald, V. N. Kalyuzhnyj, S. V. Kasilov, W. Kernbichler, and V. V. Nemov, Fusion Sci. Technol. **50**, 447 (2006).
[21] G. G. Lesnyakov, D. D. Pogozhev, Yu. K. Kuznetsov, N. T. Besedin, E. D. Volkov, and O. S. Pavlichenko, in *23rd EPS Conference on Controlled Fusion and Plasma Physics, Kiev, Ukraine, 24–28 June 1996*, edited by

D. Gresillon, A. G. Sitenko, and A. Zagorodny (European Physical Society, Mulhouse, 1996), ECA Vol. 20C, Part II, p. 547, Report b025.
[22] A. A. Subbotin, W. A. Cooper, M. Yu. Isaev, M. I. Mikhailov, J. Nührenberg, M. F. Heyn, V. N. Kalyuzhnyj, S. V. Kasilov, W. Kernbichler, V. V. Nemov, M. A. Samitov, V. D. Shafranov, and R. Zille, in *29th EPS Conference on Plasma Physics and Controlled Fusion, Montreux, Switzerland, 17–21 June 2002*, edited by R. Behn and C. Varandas (European Physical Society, Mulhouse, 2002), ECA Vol. 26B, P5.086.